European Polymer Journal 49 (2013) 4176–4188

Contents lists available at ScienceDirect

European Polymer Journal

journal homepage: www.elsevier.com/locate/europolj

Effect of spacer insertion in a commonly used dithienosilole/benzothiadiazole-based low band gap copolymer for polymer solar cells

Hussein Medlej [a], Hussein Awada [a,d], Mamatimin Abbas [b], Guillaume Wantz [b], Antoine Bousquet [a], Eric Grelet [c], Kamal Hariri [d], Tayssir Hamieh [d], Roger C. Hiorns [e], Christine Dagron-Lartigau [a,*]

[a] IPREM CNRS-UMR 5254, Université de Pau et des Pays de l'Adour, Hélioparc, 2 avenue Président Angot, 64053 Pau Cedex 9, France
[b] Université de Bordeaux, Laboratoire IMS, UMR CNRS 5218, Ecole Nationale Supérieure de Chimie, Biologie et Physique, 16 Avenue Pey Berland, 33607 Pessac Cedex, France
[c] CNRS-Université de Bordeaux, Centre de Recherche Paul-Pascal, 115 Avenue Schweitzer, 33600 Pessac, France
[d] Laboratoire de Matériaux, Catalyse, Environnement et Méthodes Analytiques (MCEMA), Campus Rafic Hariri, Hadath, Lebanon
[e] CNRS, IPREM UMR 5254, Hélioparc, 2 avenue Président Angot, 64053 Pau Cedex 9, France

ARTICLE INFO

Article history:
Received 15 June 2013
Received in revised form 23 September 2013
Accepted 25 September 2013
Available online 3 October 2013

Keywords:
Low band gap polymers
Copolymers
Organic solar cells
Polymer solar cells
Stille coupling
Microwave

ABSTRACT

Dithienosilole-benzothiadiazole based low bandgap copolymers remain promising material for organic photovoltaics. A new copolymer, poly[(4,4′-dioctyldithieno[3,2-*b*:2′,3′-*d*]silole-2,6-diyl)-*alt*-{4,7-bis[2-(3-hexyl)thienyl]-2,1,3-benzothiadiazole-5,5′-diyl}] (PDTSDTBT) was designed by introducing a thiophene spacer bearing a hexyl chain at β-position in the main backbone and compared to its analog poly[(4,4′-dioctyldithieno[3,2-*b*:2′,3′-*d*]silole-2,6-diyl)-*alt*-(2,1,3-benzothiadiazole-4,7-diyl)] (PDTSBT). In PDTSDTBT, linear alkyl chains on silicon were chosen due to facile and cheap access and the inserted 3-hexylthiophene units were chosen to increase solubility and molar mass, a weak point with PDTSBT. The two parameters are important to optimize photovoltaic performances. To compare characteristics, PDTSDTBT of molar masses greater than, and equal to a sample of PDTSBT, were prepared. Pd-catalyzed Stille cross-coupling reactions in a micro-wave reactor to promote an efficient copolymerisations. A strong absorption ranging from 370 nm to 800 nm and a good thermal stability were observed. PDTSDTBT showed better solubility and higher degree of crystallinity. Facile synthesis of high molar masses meant that higher efficiencies, around 40% greater, could be obtained with PDTSDTBT. The polymer was demonstrated to be susceptible to improvement through the use of device-additives. For example, under initial optimisations using PDTSDTBT:$PC_{60}BM$ blend at a ratio of 1:1 delivered a power conversion efficiency of 2.13% with J_{SC} = 7.73 (mA/cm^2), under AM 1.5 (100 mW/cm^2) illumination.

1. Introduction

Most of our energy is derived from fossil fuels but the supply is finite and the energy derived from the combustion of fossil fuel liberates carbon dioxide (CO_2). Providing energy from non-CO_2-emissive sources is required to prevent global warming that might induce irreversible climate change [1]. Solar energy is one of the best renewable sources of energy because of its easy access. Most commercial solar cells (photovoltaic) are made from highly purified crystal silicon [2]. Organic materials are particularly attractive because of their ease

* Corresponding author.
E-mail address: christine.dagron-lartigau@univ-pau.fr (C. Dagron-Lartigau).

0014-3057/$ - see front matter © 2013 Elsevier Ltd. All rights reserved.
http://dx.doi.org/10.1016/j.eurpolymj.2013.09.025

of processing, mechanical flexibility, and potential for low cost fabrication of large area devices. In addition, their material properties can be substantially adapted by modifying their chemical structure. The greatest understanding of the properties and photovoltaic processes has been derived from bulk-heterojunction organic solar cells (OSCs) based on poly(3-hexylthiophene) (P3HT) and [6,6]-phenyl-C_{61}-butyric acid methyl ester (PCBM) where efficiencies reached around 5% [3,4]. When seeking higher efficiencies, the deficiency of P3HT becomes apparent; its band gap at around 1.9 eV, limits absorption to values below 650 nm. By decreasing the band gap it is possible to harvest more photons (700–900 nm) and thereby increase the power conversion efficiency (PCE). Based on this point of view, the so-called low-band gap polymers have received more attention the past few years, since it is believed that they can improve the efficiency of photovoltaic devices, due to better overlap between the absorption spectra and the solar spectrum. Several recent reviews report results of a large variety of low bandgap polymers [5] and the development of fabrication techniques of large area functional organic materials [6].

The highest PCE of a low band gap polymer (based on thieno[3,4-*c*]pyrrole-4,6-dione (TPD)) reported in the literature to our knowledge is 8.5% [7], however, there are a number of industrial results which indicate that even higher values are currently being accessed [8,9]. The tuning and modification of the band gap of a conjugated polymer involves at least six factors: bond length alternation, monomer alternation, aromaticity, π-conjugation length, intermolecular interactions and inter-chain transfer [10,11]. One of the most efficient methods to decrease the band gap of conjugated polymer materials, and thereby enhance the photocurrent, is to incorporate electron rich unit (donor D) and electron deficient unit (acceptor A) in an alternating fashion in the polymer chain. The D–A system exhibits partial intramolecular charge transfer (ICT) that enables manipulation of the electronic structure (HOMO/LUMO) leading to a low band gap polymer with high charge carrier mobilities [12]. Common donor moieties include thiophene [13], carbazole [14], fluorene [15], dibenzosilole [16], dithieno[3,2-*b*:2,3-*d*]silole [17], benzo[1,2-*b*;3,4-*b*]dithiophene [18] and cyclopentadithiophene [19] groups, while acceptors moieties are usually 2,1,3-benzodiathiazole [20], diketopyrrolopyrrole [21], thieno[3,4-*b*]thiophene [22], and dioxypyrrolothiophene [18]. Among the donor units dithieno[3,2-*b*:2,3-*d*]silole (DTS)-containing polymers have attracted attention as novel systems [23–25], with high photochemical stability [26], in which the Si-C σ-orbital effectively mixes with the π-orbital of the butadiene fragment to afford a low-lying LUMO and a relatively low band gap [27]. In addition, silicon introduction stabilizes the diene HOMO level compared to the carbon counterparts, which should enhance the ambient stability of silole polymers. For example, by replacing the carbon atoms on the 9-position of the fluorene units of PFDTBT with silicon atoms, a higher efficiency of 5.4% was obtained from poly[(2,7-dioctylsilafluorene)-2,7-diyl-*alt*-(4,7-bis(2-thienyl)-2,1,3-benzothiadiazole)-5,5′-diyl] (PSiFDTBT) [16]. For the acceptor units, 2,1,3-benzothiadiazole (BT), which possess strong electron accepting features, because of the two electron withdrawing imines (C=N) and the bridged nitrogen atom, has been incorporated in a growing number of low band gap materials [20,24,28] in large part due to the ease of preparing the monomer 4,6-dibromo-2,1,3-benzothiadiazole [29]. The other possible comonomer is the 4,7-dithien-5-yl-2,1,3-benzodiathiazole (DTBT) [14,15,28,30] where there are two thiophene spacers between the BT unit and the electron-rich unit. The number of thiophenes between the benzothiadiazole units affects the band gap of the polymer [31]. It was thus possible to decrease the band-gap of polymer from 2.1 eV for one thiophene unit to 1.65 eV for four thiophene units [31]. The solubilizing side chains on a given conjugated copolymer may have considerable impact on the material properties. The chain nature (linear or branched) and the position not only fix material solubility but may also change the optoelectronic characteristics [32]. Several copolymers based on DTS and BT or DTBT were synthesized and investigate the effect of changing alkyl group's length and position. PCE obtained with copolymers based on DTS and BT were dependent on the alkyl chain present on the Si atom of the DTS unit, 4.7% with branched ethylhexyl chains [24] and 5.8% with linear dodecyl chains [20]. The studies on copolymers based on DTBT showed that a higher PCE of 3.43% [23] can be obtained with the long dodecyl chains, due to better solubility and improved π–π stacking with respect to the hexylated subunit which is poorly soluble and leads to a PCE of 0.18% [33]. On the other hand, introducing branched ethylhexyl chain leads to higher steric hindrance and lower PCE of 2.95% in comparison with dodecyl chain [23]. The presence of alkyl groups with different length and position on the acceptor unit (DTBT) is of interest: studies show that alkyl groups are better placed on thiophene spacers rather than on the BT unit [34], and indeed best placed at the thiophene β-position to minimize twisting and the consequent disruption of conjugation [35,36].

Given this understanding of the literature, we decided to synthesize two low band gap polymers poly[(4,4′-dioctyldithieno[3,2-*b*:2′,3′-*d*]silole-2,6-diyl)-*alt*-{4,7-bis[2-(3-hexyl)thienyl]-2,1,3-benzothiadiazole-5,5′-diyl}] (PDTSDTBT) and poly[(4,4′-dioctyldithieno[3,2-*b*:2′,3′-*d*]silole-2,6-diyl)-*alt*-(2,1,3-benzothiadiazole-4,7-diyl)] (PDTSBT) with linear octyl chains on the DTS unit. The aim of our work focuses on studying the effect of thiophene group bearing a hexyl side chain at β-position on the conjugation length and photovoltaic performances.

2. Experimental section

2.1. Materials

All manipulations involving air-sensitive reagents were carried out under dry nitrogen using flame-dried glassware and conventional Schlenk techniques unless otherwise stated. Syringes which were used to transfer reagents or solvents were purged with nitrogen prior to use. Chemicals and reagents were used as received from Aldrich (France) and ABCR (Germany) without further purification, unless stated otherwise. Solvents (Baker, France) were used as

received except for THF which was distilled from over sodium and benzophenone under nitrogen, and *N*,*N*-dimethylformamide (DMF) which was dried over CaH_2 under nitrogen and filtered *via* a syringe equipped with a poly(vinylidene difluoride) (PVDF) filter of 0.2 μm pore diameter.

2.2. Measurements and characterization

Nuclear magnetic resonance (NMR) spectra were recorded using a Bruker® Advance 400 MHz spectrometer in $CDCl_3$ and ambient conditions. Chemical shifts of the ^1H NMR were reported in ppm relative to the singlet of $CDCl_3$ at 7.26 ppm and coupling constants (J) are given in Hertz (Hz). All purifications were performed on a Combi*Flash*® R_f system by TELEDYNE ISCO. Flash Purification System using Redi*Sep*® *Rf* Flash Purification Cartridges as the stationary phase (Teledyne Isco, 69-2203-340). Number–average molar masses (M_n), mass–average molar masses (M_m), and dispersities ($Đ = M_m/M_n$), were estimated against polystyrene standards by gel permeation chromatography (GPC) using a bank of 4 columns (Shodex KF801, 802.5, 804 and 806) each 300 mm × 8 mm at 30 °C with THF eluant at a flow rate of 1.0 mL min^{-1} controlled by a Malvern pump (Viskotek, VE1122) and connected to Malvern VE3580 refractive index (RI) and Malvern VE3210 UV–visible detectors. Thermogravimetric analysis (TGA) was performed on a TGA Q50, TA Instruments at a heating rate of 10 °C min^{-1} under air. Differential Scanning Calorimetry (DSC) was carried out with TA Instruments Q100 operating under a nitrogen atmosphere with heating rate of 10 °C min^{-1} and cooling rate of 5 °C min^{-1}. UV–visible absorption spectra were recorded on a Shimadzu UV-2450PC spectrophotometer. X-ray diffraction experiments were performed using a Rigaku rotating anode generator at a wavelength of 1.54 Å (Cu K-alpha emission). The spectra were recorded with a bidimensional detector located at 158 mm from the sample, which was introduced as a powder in glass capillary tubes (Glas, Muller, Germany) exhibiting a diameter of 1.5 mm. All samples received a thermal annealing at 150 °C for 30 min in order to improve the grain size and the local organization of the polymers. Cyclic Voltammetry (CV): a standard three-electrode electrochemical setup (AUTOLAB PGSTAT 101) consisting of a glassy carbon or a platinium disk as working electrode (2 mm diameter), a platinum foil as counter electrode, and a AgCl/Ag as reference electrode, was used in the electrochemical experiments. At the end of each experiment performed in CH_3CN/Bu_4NPF_6 (0.1 M), the standard potential of the ferrocenium/ferrocene couple, $E_{Fc+/Fc}$, was measured, and all potentials were referenced against SCE using a previous determination of $E_{Fc+/Fc}$ = 0.41 V versus SCE in CH_3CN[37]. Polymers were drop casted from a 10 mg/mL polymer solution in chlorobenzene/Bu_4NPF_6 (0.1 M) on the working electrode. Only values from the first sweep on a film were used as the film is changed or destroyed during the first oxidation. The scan rate used was 100 mV s^{-1}. Microwave experiments were performed using a single-mode microwave reactor (CEM Discover). Microwave assisted polymerization reactions were carried out in standard Pyrex vessels (total capacity of 10 mL) sealed with Teflon septum caps. The reaction temperature, pressure, and microwave power were monitored using a computer controlled CEM-Discover focused synthesis system.

2.3. Fabrication of polymer solar cells

Organic solar cells were prepared according to the following procedure: Indium tin oxide (ITO) – coated glass electrodes (10 Ω/sq, *Kintec*), were cleaned in successive solutions of acetone, ethanol and iso-propanol for 15 min under ultrasound. After drying the substrates with air flow, UV–ozone treatment (15 min) was applied to the substrates in order to increase the hydrophilic nature of the surface and to remove residual organic contamination. A water dispersion of poly(3,4-ethylenedioxythiophene) doped with poly(styrenesulfonate) (PEDOT:PSS, *Sigma–Aldrich*) was spin-coated (4000 rpm/40 s, with about 40 nm thickness) onto the ITO sheets, followed by a thermal treatment at 110 °C for 30 min to remove residual moisture. All further device elaboration and characterizations steps were carried out under inert atmosphere (N_2) in gloveboxes. Commercially available $PC_{60}BM$ (99%, *Solaris Chem. Inc.*) and $PC_{70}BM$ (>99%, *Solaris Chem. Inc.*) were used without further purification. Solutions of polymer:PCBM (10 mg mL^{-1}) were prepared with weight ratio 1:1 and kept stirred on a hot plate at 50 °C overnight. Solutions were then spin-coated on the PEDOT:PSS layer (500 rpm/40 s) resulting in layers of 100 nm thick as indicated by an *Alpha-step IQ* profilometer. Finally, an aluminum top electrode (100 nm) was thermally evaporated under secondary vacuum (10^{-6} mbar) through a shadow mask determining the active surface (8.6 mm^2). The complete devices were annealed on a hot plate at 140 °C for 10 min in the glove box. The current density–voltage (J–V) characteristics of the cells were measured with a *Keithley 2400* under illumination using an AM1.5 solar simulator set at 100 mW/cm^2, with an *IL1400BL* calibrated radiometer. Quantum efficiencies were measured with a Xe lamp, monochromator and optical fiber focused on devices. The photocurrent was collected with a *Keithley* 6487. Photon flux was determined with an integration sphere. EQE measurements were conducted in air without encapsulation.

2.4. Synthesis of monomers and polymers

2.4.1. 3,3′-dibromo-2,2′-bithiophene (2)

To 3-bromothiophene (**1**) (10 g, 61.35 mmol) in anhydrous THF (100 mL) at −78 °C, lithium diisopropylamide (LDA) (30.68 mL, 2.0 M solution, 61.35 mmol) was added dropwise over 30 min. After the addition, the solution was stirred at the same temperature for 1 h and anhydrous $CuCl_2$ (16.4 g, 122.7 mmol) was added in one portion. The solution was allowed to stir at −78 °C for 1 h before warming to room temperature and stirring for 16 h. 200 mL Distilled water quenched the reaction. The aqueous layer was extracted with dichloromethane. The combined organic phases were washed with distilled water, dried over anhydrous Na_2SO_4 and concentrated under reduced pressure to obtain a brown solid. The residue was purified by column

chromatography using hexane and chloroform mixture (90:10) as eluent to yield a yellowish solid. Further recrystallization from ethanol yielded compound (**2**) as a white solid (6.26 g, 63%). ^{1}H NMR ($CDCl_3$, 400 MHz) δ: 7.41 (d, ^3J = 5.4 Hz, 2H), 7.08 (d, ^3J = 5.4 Hz, 2H).

*2.4.2. 3,3′-di-n-octylsilylene-2,2′-bithiophene (**3**)*

n-BuLi (2.5 M solution in hexane, 1.92 mL, 4.8 mmol) in anhydrous THF (45 mL) was cooled to −78 °C and 3,3′-dibromo-2,2′-bithiophene (**2**) (0.78 g, 2.4 mmol) in dry THF (15 mL) was added dropwise. The solution was stirred for 2 h and then dichlorodioctylsilane (1 g, 3.07 mmol) in 15 mL of dry THF was added dropwise at −78 °C. The reaction was stirred for 6 h at room temperature prior to quenching with saturated aqueous NH_4Cl solution (50 mL). The aqueous layer was extracted with diethyl ether, organic phases were combined and washed with water and dried over anhydrous Na_2SO_4. Filtration and evaporation of solvent gave a crude product that was purified by flash chromatography using petroleum ether as eluent to yield a light yellow oil (0.61 g, 61%). ^{1}H NMR ($CDCl_3$, 400 MHz) δ: 7.19 (d, ^3J = 4.6 Hz, 2H), 7.04 (d, ^3J = 4.6 Hz, 2H), 1.32–1.43 (m, 4H), 1.13–1.32 (m, 20H), 0.8–0.94 (m, 10H).

*2.4.3. 5,5′-Bis(trimethylstannyl)-3,3′-di-n-octylsilylene-2,2′-bithiophene (**M1**)*

To a solution of 3,3′-di-n-octylsilylene-2,2′-bithiophene (**3**) (0.39 g, 0.931 mmol) in anhydrous THF (8 mL), n-butyllithium in hexane (2.5 M, 0.93 mL, 2.328 mmol) was added slowly at −20 °C under nitrogen. The mixture was allowed to warm to room temperature and stirred for 1 h leading to the formation of a white suspension. It was then subsequently cooled to −20 °C where a 1 M solution of trimethyltinchloride (2.8 mL, 2.8 mmol) in anhydrous THF (5 mL) was added dropwise. The mixture was left to reach ambient temperature and stir overnight before being poured into deionized (DI) water. Extraction was performed using diethyl ether and repeated washing with water. Drying over anhydrous Na_2SO_4, filtering and solvent evaporation gave a crude product that was placed under high vacuum for 24 h to yield a yellow–brown viscous oil (**M1**) (0.68 g, 98%) which was used in the next step without further purification. ^{1}H NMR ($CDCl_3$, 400 MHz) δ: 7.08 (d, $^3J_{H-Sn}$ = 24.7 - Hz, 2H), 1.35–1.45 (m, 4H), 1.15–1.33 (m, 20H), 0.82–0.92 (m, 10H), 0.38 (d, $_3J_{H-Sn}$ = 56 Hz, 18H).

*2.4.4. 4-hexyl-2-trimethylstannylthiophene (**5**)*

LDA (2.0 M solution, 6.24 mL, 12.48 mmol) was added dropwise over 15 min to a solution of 3-hexylthiophene (**4**) (2 g, 11.88 mmol) in anhydrous THF (80 mL) at −78 °C. The mixture was stirred at room temperature for 1 h. After cooling again to −78 °C, a solution of trimethyltinchloride (1.0 M in THF, 13.7 mL, 13.7 mmol) was added slowly. After stirring at room temperature for overnight, the reaction was quenched by addition of 80 mL of distilled water. The mixture was then recovered with diethyl ether, and washed and dried as **M1**. The final product (**5**) was obtained as an oily liquid and used in the next step without further purification (yield: 82%). ^{1}H NMR ($CDCl_3$, 400 MHz) δ: 7.2 (d, $^4J_{H-Sn}$ = 12.2 Hz, 1H), 7.01 (d, $^3J_{H-Sn}$ = 25.6 Hz, 1H), 7.04 (s, 2H), 2.64 (t, ^3J = 7.8 Hz, 2H), 1.63 (q, 2H), 1.24–1.4 (m, 6H), 0.89 (t, ^3J = 6.8 Hz, 3H), 0.35 (d, $^2J_{H-Sn}$ = 56 Hz, 9H).

*2.4.5. 4,7-bis(4-hexylthiophen-2-yl)-2,1,3-benzothiadiazole (**6**)*

$Pd(PPh_3)_2Cl_2$ (0.09 g, 0.125 mmol) was added to a solution of 4,7-dibromo-2,1,3-benzothiadiazole (**M2**) (0.92 g, 3.12 mmol) and 4-hexyl-2-trimethylstannylthiophene (**5**) (3.1 g, 9.36 mmol) in 45 mL of anhydrous THF. The mixture was refluxed (70–80 °C) under N_2 for 24 h. The solvent was evaporated and the residue recovered with chloroform, washed with distilled water, dried over anhydrous Na_2SO_4, filtered and evaporated. The crude product was purified by flash chromatography using petroleum ether as eluent to give an orange solid (**6**) in a very high yield (98%). ^{1}H NMR ($CDCl_3$, 400 MHz) δ: 7.98 (d, ^5J = 0.6 Hz, 2H), 7.83 (s, 2H), 7.04 (d, ^5J = 0.6 Hz, 2H), 2.69 (t, ^3J = 7.8 Hz, 4H), 1.7 (q, 4H), 1.28–1.45 (m, 12H), 0.9 (t, ^3J = 7 Hz, 6H).

*2.4.6. 4,7-bis(5-bromo-4-hexylthiophen-2-yl)-2,1,3-benzothiadiazole (**M3**)*

To a solution of 4,7-bis(4-hexylthiophen-2-yl)-2,1,3-benzothiadiazole (**6**) (0.6 g, 1.28 mmol) in anhydrous DMF (33 mL) was added *N*-bromosuccinimide (NBS) (0.47 g, 2.92 mmol) in two portions. The reaction mixture was stirred at room temperature for 16 h in the dark. The resulting solution was poured into water (120 mL) and diethyl ether (120 mL) and stirred for 2 h. The organic layer was separated and washed two times with a saturated aqueous solution of sodium chloride (brine). The combined organic phase was dried over anhydrous Na_2SO_4 and filtered. The ether was removed under reduce pressure and the crude product was purified by flash chromatography using a mixture of hexane and chloroform (95/05) as eluent to give an orange solid (**M3**) in 94% yield. ^{1}H NMR ($CDCl_3$, 400 MHz) δ: 7.77 (s, 2H), 7.76 (s, 2H), 2.64 (t, ^3J = 7.7 Hz, 4H), 1.67 (q, 4H), 1.29–1.45 (m, 12H), 0.9 (t, ^3J = 7 Hz, 6H).

*2.4.7. Poly[(4,4′-dioctyldithieno[3,2-b:2′,3′-d]silole-2,6-diyl)-alt-{4,7-bis[2-(3-hexyl)thienyl]-2,1,3-benzothiadiazole-5,5′-diyl}] (**PDTSDTBT-P2**)*

In a 10 mL high pressure microwave reactor tube equipped with a sealed septum, a solution of 5,5′-bis(trimethylstannyl)-3,3′-di-n-octylsilylene-2,2′-bithiophene (**M1**) (100 mg, 0.134 mmol) and 4,7-bis(5-bromo-4-hexylthiophen-2-yl)-2,1,3-benzothiadiazole (**M3**) (80 mg, 0.128 mmol) was taken in anhydrous chlorobenzene (2 mL) in the glovebox. To the solution, tris(dibenzylideneacetone) dipalladium(0) (2.34 mg, 2 mol%), tri(o-tolyl)phosphine (3.12 mg, 8 mol%), and CuO (10.18 mg, 0.128 mmol) were added. The tube was subjected to the following conditions in a microwave reactor: 120 °C for 5 min, 140 °C for 5 min and 170 °C for 45 min. After cooling to room temperature, the resulting viscous liquid was dissolved in hot chlorobenzene then added slowly into a vigorously stirred cold methanol. The solid was subjected to Soxhlet extraction with methanol, acetone, and chlorobenzene in that order. The chlorobenzene fraction was concentrated and precipitated from methanol, and the precipitant was filtered and

dried under reduced pressure to afford **PDTSDTBT-P2**, as a dark-blue solid. The yield of the polymerization reaction was 88%. GPC: M_w = 35,800 g mol^{-1}, $Đ$ = 2.28.

2.4.8. Poly[(4,4′-dioctyldithieno[3,2-b:2′,3′-d]silole-2,6-diyl)-alt-{4,7-bis[2-(3-hexyl)thienyl]-2,1,3-benzothiadiazole-5,5′-diyl}] (PDTSDTBT-P1)

A second batch of **PDTSDTBT** prepared under similar conditions except that the reactor tube was subjected to the following conditions in the microwave reactor: 120 °C for 5 min, 140 °C for 5 min and 170 °C for 15 min. **PDTSDTBT-P1**: M_w = 8500 g mol^{-1}, $Đ$ = 1.29.

2.4.9. Poly[(4,4′-dioctyldithieno[3,2-b:2′,3′-d]silole-2,6-diyl)-alt-(2,1,3-benzothiadiazole-4,7-diyl)] (PDTSBT-P3)

The polymerization process was the same as that for **PDTSDTBT-P1**, except that 4,7-dibromo-2,1,3-benzothiadiazole (**M2**) co-monomer was used instead of monomer (**M3**). The polymer was extracted using Soxhlet apparatus with methanol, acetone, hexane, and chlorobenzene. The chlorobenzene fraction was concentrated and precipitated into methanol, and the precipitant was filtered and dried under reduced pressure to afford **PDTSBT-P3**, as a metallic shine solid. GPC: M_w = 7700 g mol^{-1}, $Đ$ = 1.35.

3. Results and discussion

3.1. Synthesis of monomers

The synthetic route of 5,5′-bis(trimethylstannyl)-3,3′-di-*n*-octylsilylene-2,2′-bithiophene (**M1**) is shown in Scheme 1, and begins with commercially available 3-bromothiophene (**1**). This was selectively lithiated in the 2 position using lithium diisopropylamide (LDA). The resulting anion, stabilized by the inductive effect of the bromine atom, was oxidatively dimerized by treatment with $CuCl_2$ to afford the head-to-head coupled dimer (**2**) in 63% yield. Double lithiation of 2,2′-dibromobithiophene (**2**) with *n*-BuLi at −78 °C, followed by subsequent quenching with the corresponding dioctyldichlorosilane (Oct_2SiCl_2), yields 3,3′-di-*n*-octylsilylene-2,2′-bithiophene (**3**) as light-yellow oil in 60% yield. This compound is light-sensitive: it converted to a viscous blue oil on standing for a few days in light. Compound (**3**) was then further selectively lithiated with *n*-BuLi at the α-positions and protected with trimethyltin groups to produce monomer **M1**. The di-trimethylstannyl compounds proved unstable in all types of column purification included silica and neutral or basic alumina [38]. Therefore, the obtained crude product was dried under high vacuum to remove the excess of Me_3SnCl, providing a pale yellow oil in a very high yield (~98%).

The synthesis of 4,7-dibromo-2,1,3-benzothiadiazole monomer (**M2**) has been done following procedure reported in the literature [29]. The thiophene-benzothiadiazole comonomer (**M3**) was synthesized by adopting the procedure illustrated in Scheme 2. In this procedure, selective deprotonation of 3HT (**4**) in 5 position has been performed by the addition of one equivalent of LDA base at low temperature. This step is followed by *in situ* reaction of the lithium salt with trimethyltin chloride (Me_3SnCl) provided the corresponding 4-hexyl-2-trimethylstannylthiophene (**5**) in 82% yield. Note that the lithiation of 3-hexylthiophene using *n*-BuLi/TMEDA [39] and following by the addition of Me_3SnCl get a mixture of 2- and 5-functionalized 3-hexylthiophene. The formation of undesirable 2-stannyl-3-hexythiophene may be due to the less steric hindrance of *n*-BuLi in comparison with LDA allowing access to the 2-position. The synthesized thiophene-stannyl compound (**5**) was then reacted with 4,7-dibromo-2,1,3-benzothiadiazole (**M2**) by Stille cross-coupling reaction. This reaction proceeded in the presence of 4 mol% of $Pd(PPh_3)_2Cl_2$ as catalytic system providing the 4,7-bis(4-hexylthiophen-2-yl)-2,1,3-benzothiadiazole (**6**) in very high yield (98%). Compound (**6**) was dibrominated using NBS in DMF to give dibromo-functionalized comonomer (**M3**) as orange solid with 94% yield.

3.2. Polymer synthesis

General synthetic strategy for **PDTSBT** and **PDTSDTBT** copolymers is outlined in Scheme 3. The BT-based polymer **PDTSBT-P3** was synthesized by microwave-assisted Stille cross-coupling polymerization [40] using the corresponding monomers **M1**/**M2** and $Pd_2(dba)_3$/P(o-Tol)$_3$/CuO as the catalyst system in chlorobenzene. Since the palladium catalyst is sensitive to light, the polymerization was run in the dark. **PDTSBT-P3** exhibited an M_n of 5700 g mol^{-1}, with a low dispersity of 1.35, as indicated by gel permeation chromatography (GPC) against polystyrene standards. This polymer is soluble in chlorinated solvents, such as $CHCl_3$, chlorobenzene (CB) and dichlorobenzene (DCB). **PDTSDTBT** copolymers were synthesized by the same method using 5,5′-bis(trimethylstannyl)-3,3′-di-n-octylsilylene-2,2′-bithiophene (**M1**) and the appropriate dibromo compound (**M3**) in chlorobenzene; the polymers comprised the DTS and DTBT units. To evaluate the effect of the molar mass on the optoelectronic properties and device performance, two **PDTSDTBT** polymers were synthesized, namely **PDTSDTBT-P1** with a M_n of 6600 g mol^{-1} and **PDTSTDBT-P2** with a higher M_n of 15,700 g mol^{-1}

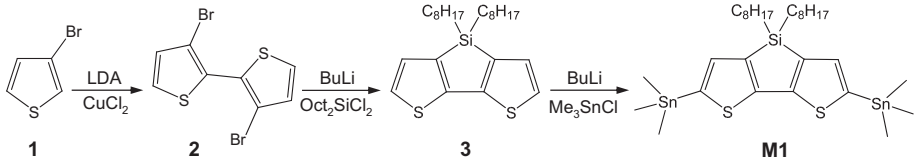

Scheme 1. Synthetic route and molecular structure of the monomer **M1**.

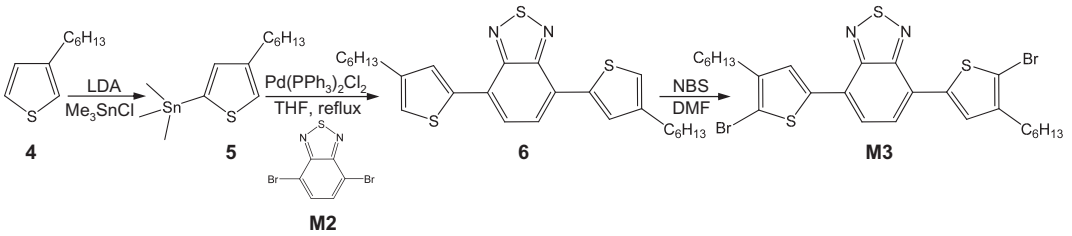

Scheme 2. Synthetic route and molecular structure of the monomer **M3**.

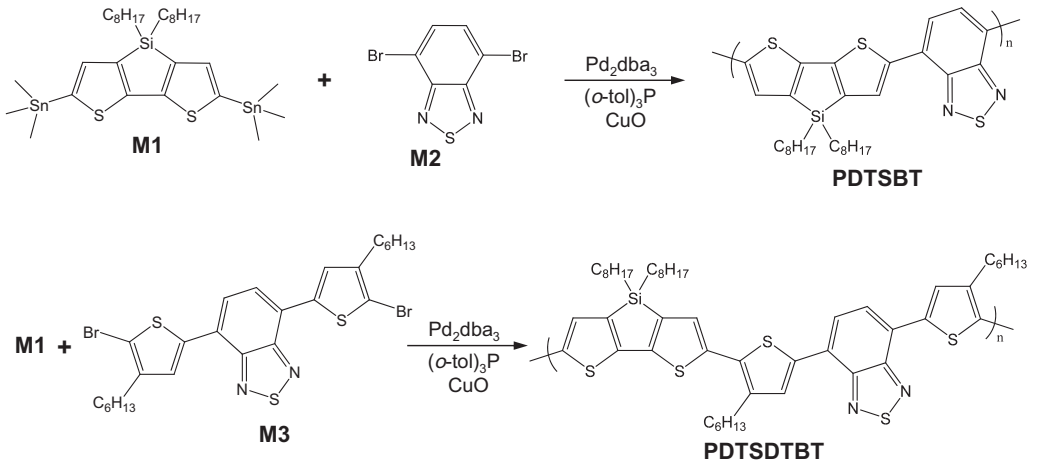

Scheme 3. Synthetic route and molecular structure of **PDTSBT** and **PDTSDTBT** copolymers.

Table 1
Molar masses and temperature of thermal degradation of the copolymers.

Polymers	M_m [a] (g mol^{-1})	M_n [a] (g mol^{-1})	$Đ$ [a]	T_5 (°C) [b]
PDTSDTBT-P1	8500	6600	1.29	368
PDTSDTBT-P2	35,800	15,700	2.28	–
PDTSBT-P3	7700	5700	1.35	362

[a] M_n, M_m and $Đ$ determined by GPC against polystyrene standards.
[b] T_5: temperature corresponding to a 5% weight-loss under air.

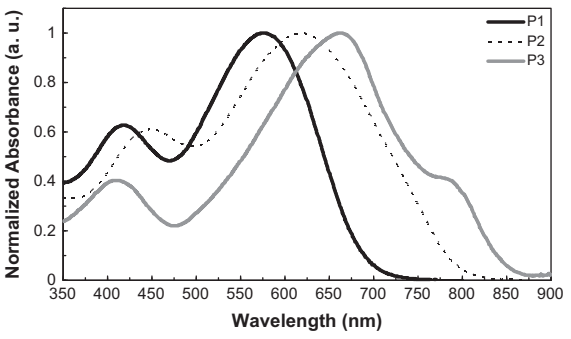

Fig. 1. Normalized UV–visible absorption spectra of **P1**, **P2** and **P3** in $CHCl_3$ solution.

(Table 1). Both copolymers were readily soluble in common organic solvents and had greater solubility in comparison with **PDTSBT-P3** especially in THF and chloroform.

3.3. Optical properties

Fig. 1 presents the absorption spectra of the copolymers recorded from $CHCl_3$ solutions at room temperature. The corresponding data are summarized in Table 2.

The solution absorption spectra of **PDTSDTBT** (**P1** and **P2**) and **PDTSBT** (**P3**) showed similar profile with two significant absorption peaks. The first absorption band is situated at short wavelengths and attributed to the π–π^* electronic transition of dithienosilole unit, while the second at higher wavelengths can be assigned to the internal charge transfer (ICT) interaction between the electron-accepting **BT** and electron-donating **DTS** or **HT** units [41,42]. Moreover, a vibronic shoulder appeared only in the case of **PDTSBT** (**P3**) at 784 nm implying that a certain degree of π–π aggregation was already occurring in solution [43]. The presence of this shoulder can explain the lower solubility of this copolymer compared to **P1** and **P2**. Looking closer the absorption spectra of the two **PDTSDTBT** copolymers, an important red-shift of 44 nm of the absorption band can be observed passing from **P1** to **P2**. This bathochromic shift can be attributed to the molar mass of **P2** (15,700 g mol^{-1}) higher than that of **P1** (6600 g mol^{-1}). The increase in molar mass results in an increase of the conjugation length and shifting the absorption spectrum to higher wavelengths. On the other hand, to compare the optical properties of the two types of copolymers **PDTSDTBT** and **PDTSBT**, we take the case of **P1** (M_n = 6600 g mol^{-1}) and **P3** (M_n = 5700 g mol^{-1}) having

Table 2
Optical properties of the polymers (bold values correspond to the wavelength at the maximum of absorption).

Polymers	Solution[a] λ_{max} (nm)	Film[b]		
		λ_{max} (nm)	λ_{onset} (nm)	E_g^{opt} (eV)[c]
P1	420, **576**	461, **649**	794	1.56
P2	452, **620**	467, **673**	815	1.52
P3	412, **664**, 784	430, **689**, 78	856	1.44

[a] In dilute chloroform solution.
[b] Spin-coated from CB solution.
[c] Optical band gap estimated from the low energy band edge in the optical spectrum, $E_g^{opt} = 1240/\lambda_{onset}$.

approximately the same degree of polymerization. The absorption spectra of **P1** and **P3** show that the addition of the hexylthiophene units in **PDTSDTBT** did not affect substantially the position of the high-energy band. However, the low-energy band is blue-shifted by 88 nm. This hypsochromic shift may indicate the presence of a twist between thiophene and dithienosilole units which is induced by hexyl side chains. Moreover, the addition of hexylthiophene units leads to a less pronounced coupling between the donor and the acceptor units, reducing intramolecular charge transfer and increasing the band gap.

The optical properties of **P1**, **P2** and **P3** were also studied in the solid state. The thin films were spin-coated from solutions in chlorobenzene and then annealed at 140 °C for 15 min. Fig. 2 shows the absorption spectra of the polymer films and Table 2 lists the optical properties of the copolymers.

Similarly to what was observed in solution, the absorption spectra in solid state are affected by the molar mass and the chemical structure of the copolymers. Compare to solution, the absorption spectra of the thin films show broader absorption bands, the red-shift of these absorptions bands indicates a strong intermolecular interaction in the solid state [44]. Moreover, in the case of **P3**, the intensity of the vibronic shoulder in the solid state was increased significantly relative to that in solution, indicating that much stronger interchain π–π stacking occurred in the solid state. The absorption edges (λ_{onset}) of the three polymer films are

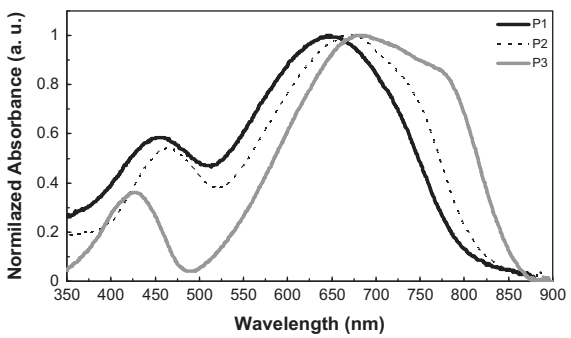

Fig. 2. Normalized UV–visible absorption spectra of **P1**, **P2** and **P3** spin-coated thin films from chlorobenzene solutions.

794 nm for **P1**, 815 nm for **P2** and 856 nm for **P3**, from which the optical bandgaps (E_g^{opt}) of the polymers can be estimated according to $E_g^{opt} = 1240/\lambda_{onset}$. The E_g^{opt} values of **P1**, **P2** and **P3** are 1.56, 1.52 and 1.44 eV, respectively. **PDTSBT-P3** possessed the lowest band gap due to electron-rich dithienosilole donor units in direct combination with benzothiadiazole acceptor units promoting better planarity of the backbone and an efficient intra-molecular charge transfer in comparison with **P1** and **P2**. In the case of **PDTSDTBT**, the optical band gap of **P2** is smaller than the one for **P1**, in correspondence to its red-shifted absorption edge and its higher chain length due to the higher molar mass.

3.4. Thermal properties

Thermal stability of **PDTSDTBT** and **PDTSBT** was investigated by thermogravimetric analyses (TGA). The analyses were performed under air between 30 and 800 °C, as shown in Supporting Information Fig. S1. The temperature of 5% weight-loss was selected as the onset point of degradation (T_5). The T_5 values of **PDTSDTBT** and **PDTSBT** are 368 and 362 °C, respectively, indicating that they have an excellent thermal stability for the applications in optoelectronic devices. The very high thermal stability of these polymers can be attributed to the presence of the aromatic ring dithieno[3,2-*b*:2′,3′-*d*]silole rich in silicon in the polymer backbone. Note that the thermal stability of **PDTSDTBT** with a thiophene unit inserted between **BT** and **DTS** units is higher than that of the **PDTSBT**, maybe due to the increase of the molar mass in **PDTSDTBT**.

The TGA plots of the copolymers show two steps of thermal decomposition between 300 °C and 700 °C. The first step start from the onset decomposition temperature up to 550 °C and 520 °C in the case of **PDTSDTBT** and **PDTSBT** respectively, this step can be attributed to the loss of the alkyl side chains. The second process of degradation took place at 520–700 °C and was most likely due to the degradation of the polymer main chain.

The thermal properties of the two copolymers were also evaluated by Differential Scanning Calorimetry (DSC). The analyses were carried out under nitrogen atmosphere in a temperature range from −50 °C to 300 °C. The DSC curves and the characteristic temperatures of these copolymers were recorded in the second cycle and are shown in Supporting Information, Fig. S2.

Up to 300 °C, the DSC curve of **PDTSBT** did not show any major thermal phenomenon. In the case of **PDTSDTBT**, the DSC thermogram clearly shows an endothermic transition during the temperature rise, corresponding to a glass transition temperature (T_g) at around 30 °C. This transition is probably due to the movements of hexyl side chains on thiophene units upon heating at this temperature.

The absence of melting and crystallization peaks in the two polymers can have two explanations. Either a low crystallinity of both materials due to insufficient flatness preventing the necessary stacking of the polymer chains at long distance to form crystalline regions, or, the backbone rigidity and the strong interchain interactions induced by the dithienosilole units can lead to melting

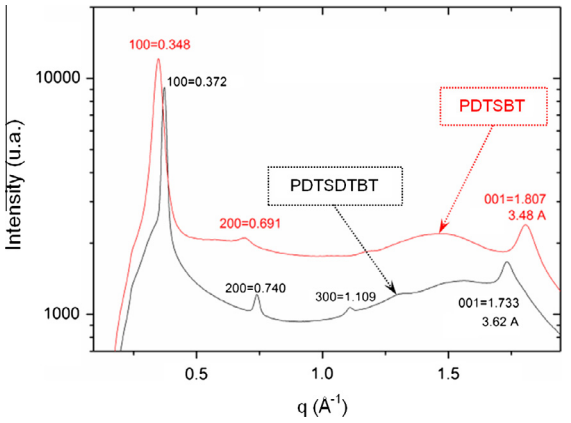

Fig. 3. Powder X-ray diffraction spectra of **PDTSDTBT** (**P1**) and **PDTSBT** (**P3**).

temperatures above the limit temperature of 300 °C. Similar observations in low band copolymers based on dithieno[3,2-*b*:2′,3′-*d*]silole and thieno[3,4-*c*]pyrrole-4,6-dione units have been reported by Yuan et al. [45].

3.5. Structural properties

X-ray diffraction measurement was performed on **PDTSDTBT** and **PDTSBT** powders after annealing at 150 °C for 30 min, the diffractograms are shown in Fig. 3. **PDTSBT** exhibit a distinct peak at 0.348 $Å^{-1}$ corresponding to the reflection of (100) crystalline plane with an interlayer spacing d_{100} of 18 Å. The 18 Å d_{100} value is typical for the octyl groups separating the main chains. The (001) crystal planes, which are oriented perpendicularly to the (100) planes, are also detected with a distance d_{001} (π-stacking spacing) estimated at 3.48 Å. This value is very close to the reported d_{001} for the same polymer with 2-ethyhexyl chains on dithienosilole units [46]. To the best of our knowledge, this short distance was not observed in other semiconducting self-assembled polymers, for example, d_{001} of P3HT is approximately 3.8 Å [47,48]. The strong stacking of **PDTSBT** molecules leads to limited solubility in organic solvents and explains the UV–visible results of this polymer obtained in chloroform solution (shoulder at 778 nm). It is interesting to note that the XRD spectra of **PDTSBT** also shows a wide diffraction peak centered at about 1.46 $Å^{-1}$ and corresponding to a spacing distance (d) of 4.3 Å. The 4.3 Å spacing could be attributed to the lateral short-range order of the molten octyle chains suggesting that these chains are not extended as observed in the case of P3HT [49].

The XRD spectra of **PDTSDTBT** copolymer showed diffraction peaks at 0.372, 0.74 and 1.109 $Å^{-1}$ which correspond to an interlayer distance (d) of 16.9 Å. This distance is smaller than that of the **PDTSBT** copolymer (18 Å) and it is probably responsible for obtaining of higher order diffraction peaks, more intense and more defined. The presence of the diffraction peaks up third order in this polymer shows a crystallinity greater than that of **PDTSBT**. Another diffraction peak at 1.733 $Å^{-1}$ was observed in the (001) crystalline plane, which could be assigned to a π–π stacking distance (d_{001}) of 3.62 Å. This distance is higher than that obtained in the case of **PDTSBT** (3.48 Å) suggesting a twist in the main chain due to the steric effect induced by hexyl side chains of thiophene units. These observations suggest that the twist of the thiophene rings leads to shorter interlayer distance and poor packing of thiophene rings in **PDTSDTBT** polymer.

3.6. Electrochemical measurements

The electrochemical cyclic voltammetry was performed to determine the HOMO and the LUMO energy levels of the conjugated polymers. Fig. 4 shows the cyclic voltammograms (CVs) of the **PDTSBT** and **PDTSDTBT** films on platinum disc electrode in 0.1 mol/L Bu_4NPF_6 chlorobenzene solution. Clearly, both copolymers have reversible *p*-doping/*n*-doping processes in the positive and negative scanning ranges. The onset reduction potentials (E_{red}) of **PDTSBT** and **PDTSDTBT** are −1.24 and −1.18 V versus SCE, respectively, while the onset oxidation potentials (E_{ox}) are 0.55 and 0.65 V versus SCE, respectively (see Table 3). These potentials are determined using the tangent method (see Figs. S3 and S4 in Supporting information).

HOMO and LUMO energy levels can be estimated using the empirical equations: $E_{HOMO} = -(E_{ox} + 4{,}7)$ and $E_{LUMO} = -(E_{red} + 4{,}7)$, where 4,7 is the scale factor connecting SCE to vacuum [50]. The two polymers have slightly different LUMO energy levels that were determined to be −3.52 eV (**PDTSDTBT**) and −5.46 eV (**PDTSBT**). And the HOMO energy levels of **PDTSDTBT** and **PDTSBT** are −5.35 and −5.25 eV, respectively. The 0.1 eV difference between the HOMO energy levels of the two polymers is attributed to the addition of hexylthiophene ring in **PDTSDTBT** polymer. The electrochemical bandgaps (E_g^{ec}) of **PDTSDTBT** and **PDTSBT** copolymers, estimated from the difference between the onset potential for oxidation and reduction, are respectively 1.83 and 1.79 eV; the values are larger than their optical bandgaps (1.52 and 1.44 eV, respectively). Such similar difference between the electrochemical and optical bandgap has been observed in studies of other D–A polymers presumably resulting from the interface barrier for charge injection.

Table 3
Electrochemical properties of the polymers.

Polymers	E_{ox} (V)[a]	E_{red} (V)[a]	E_{HOMO} (eV)[b]	E_{LUMO} (eV)[b]	E_g^{ec} (eV)[c]
PDTSDTBT	0.65	−1.18	−5.35	−3.52	1.83
PDTSBT	0.55	−1.24	−5.25	−3.46	1.79

[a] Measured on the film of the polymers casted on a Pt electrode in acetonitrile with 0.1 M Bu_4NPF_6.
[b] Calculated using the following equation: $E_{HOMO,LUMO} = -(E_{ox,red} + 4{,}7)$.
[c] The difference between the onset potentials of oxidation and reduction.

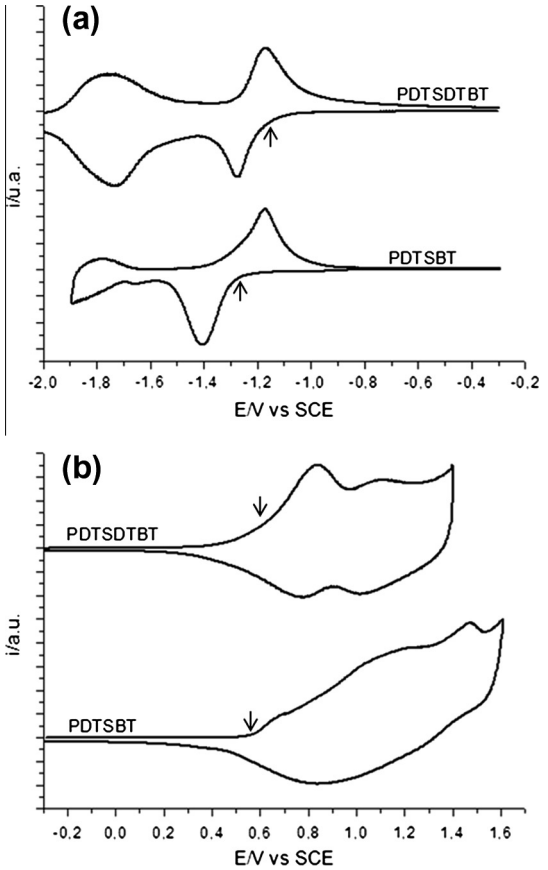

Fig. 4. Cyclic Voltammetry curves (a) reduction and (b) oxidation waves of polymer films performed in 0.1 M Bu_4NPF_6/CH_3CN using a sweep rate of 100 mV s^{-1}. The arrows show the onset potentials.

3.7. Photovoltaic properties

To investigate and compare the photovoltaic properties of the both copolymers, bulk heterojunction PSC devices with a configuration of ITO/PEDOT:PSS/**PDTSDTBT** or **PDTSBT**:$PC_{70}BM$/Al were fabricated from an active layer where, copolymers were blended with $PC_{70}BM$ in a weight ratio of 1:1 w/w in chlorobenzene solutions and spin coated on ITO/PEDOT:PSS substrates. All devices were annealed at an optimized temperature of 140 °C for 10 min and tested under simulated AM 1.5 G irradiation (100 mW/cm^2). $PC_{70}BM$ was chosen initially as the acceptor because it possesses strong absorption in the visible region from 440 to 530 nm appealing to low band gap polymers [51]. *J–V* curves for P1, P2 and P3 are shown in Fig. 5a, indicating a strong difference between the curves for these three samples. The corresponding open-circuit voltage (V_{OC}), short-circuit current density (J_{SC}), fill factor (FF), and power conversion efficiency (PCE) of the cells are summarized in Table 4. Because of the slight difference in the HOMO levels of the copolymers, they exhibited similar V_{OC} values (0.50–0.52 V), and thus the PCEs were dependent on their J_{SC} and FF values.

The PSCs based on **PDTSDTBT** (**P1**) (M_n = 6600 g mol^{-1}, $Đ$ = 1.29) demonstrates a short-circuit current (J_{SC}) of 3.58 mA cm^{-2}, an open-circuit voltage (V_{OC}) of 0.5 V, a fill factor (FF) of 34%, and PCE of 0.61%. However, an optimized photovoltaic performance with a J_{SC} of 6.98 mA/cm^2, a V_{OC} of 0.52 V, a FF of 39%, and an overall PCE of 1.41% has been achieved under same conditions for the other batch of **PDTSDTBT** (**P2**) (M_n = 15,700 g mol^{-1}, $Đ$ = 2.28). The significant improvement in the PV performance, observed with the high-molar mass **PDTSDTBT**, is mainly due to the enhancement of the J_{SC} caused by increasing of the conjugation lengths and consequently the amelioration of the optical properties. In addition, this optimization was not only due to the optical properties, but also could be due to the improvement of charge carrier mobility and the morphology at the nanoscale level of the BHJ film as demonstrated earlier [52].

After studying the effect of the molar mass of **PDTSDTBT** on the photovoltaic characteristics, we also compare the performance of the two types of copolymers (**PDTSDTBT** and **PDTSBT**), for this, only **P1** was considered, as it exhibits a molar mass similar to that of **P3** (M_n = 5700 g mol^{-1}). The devices prepared from **P3**:PC_{70}BM exhibited an equivalent V_{OC} of 0.5 V, a higher J_{SC} of 5.33 mA.cm^{-2}, and a higher FF of 38%, resulting in an overall PCE of 1.01%. The better photovoltaic performance of **P3** results from its higher J_{SC} and FF, which is probably due to better overlap of its absorption spectrum with solar spectrum. Indeed, the addition of hexylthiophene group in **P1** twists the backbone, decreases π-π stacking interaction and also reduces the intramolecular charge transfer resulting in a decrease of the current density of the device and its power conversion efficiency. Moreover, it is difficult to compare these results to the previous ones reported in the literature on analogous copolymers (with dodecyl chains) [20,23] as the molecular weights of P1 and P3 are low and could be an explanation of weak performances. Devices with **P3** could not excel in performance than the ones with **P2**, due to lower molar mass. Therefore, our follow-up studies are based on the best performing polymer **P2**.

In order to further enhance the PSC device performance with **P2**, both pre-annealing and post-annealing treatment were carried out and *J–V* curves of the devices are shown in Fig. 5b. Pre-annealing (140 °C/10 min) was intended to optimize donor/acceptor phase separation, while post-annealing (150 °C/10 min) was mainly aimed for achieving optimum active layer/metal interface. Moreover, devices with $PC_{60}PM$ as acceptor were also investigated, as **P2** seems to have very wide absorption pattern including the lower visible part. The device with $PC_{60}PM$ performed better than the device with $PC_{70}PM$ with PCE of 1.94% versus 1.79%. Device performance parameters are shown in Table 5. Higher J_{SC} and V_{OC} in the devices prepared from PC_{60}PM can be due to higher mobility of $PC_{60}PM$ resulting in faster charge transport and weaker recombination. Slightly higher FF in the devices prepared from $PC_{70}PM$ is due to lower series resistance coming probably from better film morphology.

Fig. 6 (lower panel) displays the external quantum efficiency (EQE) curves of these devices showing extended current generation up to 800 nm and well corroborating with the absorption pattern (Fig. 6 upper panel). The

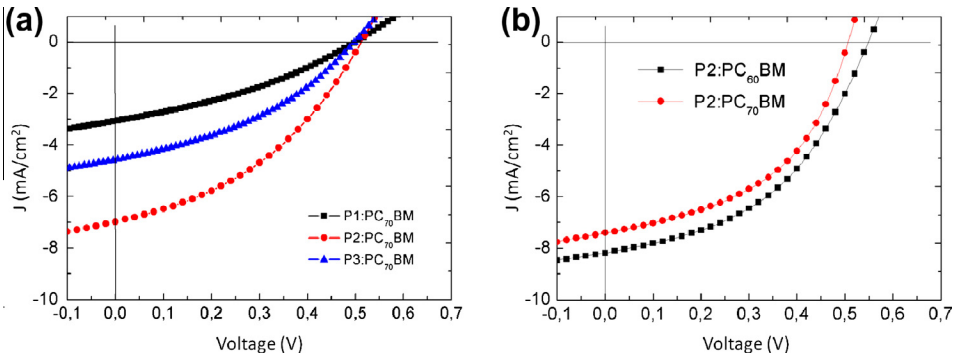

Fig. 5. (a) Illuminated *J–V* characteristics of solar cells using ITO/PEDOT:PSS/**P1**:$PC_{70}BM$ or **P2**:$PC_{70}BM$ or **P3**:$PC_{70}BM$/Al device architecture. Devices with post processing thermal treatment at 140 °C (10 min). (b) *J–V* curves of PSC based on **P2**:$PC_{60}BM$ or **P2**:$PC_{70}BM$, devices are both pre and post-annealed (140 °C for 10 min and 150 °C for 10 min, respectively).

Table 4
Photovoltaic properties of PSCs based on **PDTSDTBT** (**P1** and **P2**):$PC_{70}BM$ and **PDTSBT** (**P3**):$PC_{70}BM$.

Active layer (w/w ratio)	M_n (kg mol^{-1})	PCE (%)	J_{SC} (mA cm^{-2})	V_{OC} (V)	FF (%)
P1: $PC_{70}BM$ (1:1)	6.6	0.61	3.58	0.50	34
P2: $PC_{70}BM$ (1:1)	15.7	1.41	6.98	0.52	39
P3: $PC_{70}BM$ (1:1)	5.7	1.01	5.33	0.50	38

Table 5
Device performance parameters of PSCs (ITO/PEDOT:PSS/**P2**:$PC_{60}BM$ or **P2**:$PC_{70}BM$/Al) under AM1.5 solar illumination.

Active layer (w/w ratio)	PCE (%)	J_{SC} (mA cm^{-2})	V_{OC} (V)	FF (%)
P2: $PC_{60}BM$ (1:1)	1.94	7.94	0.56	44
P2: $PC_{70}BM$ (1:1)	1.79	7.40	0.50	48

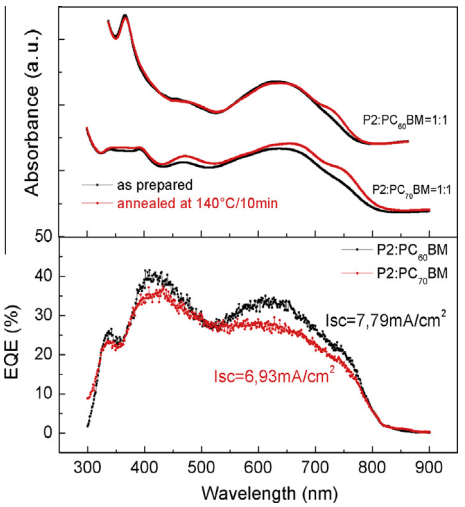

Fig. 6. (upper panel) Absorption spectra of **P2**:$PC_{60}BM$ and **P2**:$PC_{70}BM$ films before and after annealing at 140 °C/10 min; (lower panel) External quantum efficiency (EQE) spectra of the polymer solar cells (ITO/PEDOT:PSS/ = **P2**:$PC_{60}BM$ or **P2**:$PC_{70}BM$/Al).

short-circuit current density obtained from integrating EQE curves of the devices based on **P2**:$PC_{60}BM$ and **P2**:$PC_{70}BM$ are 7.79 and 6.93 mA/cm^2, respectively, which reasonably agrees with the measured J_{SC} of 7.94 and 7.4 mA/cm^2 under the illumination of AM1.5, 100 mW/cm^2. For this reason, we continued our study using $PC_{60}BM$ as an acceptor; this point is quite interesting as $PC_{60}BM$ is also less expensive.

3.8. Effect of the additives on PDTSDTBT-P2

The morphological evolution in BHJ solar cells is crucial for their performance and it has been reported that the addition of the process additives to the blend solution before spin-coating into the films significantly affects the efficiency of the resulting organic solar cell performance [53]. Herein, we tried 1,8-diiodooctane (DIO) and 1-chloronaphthalene (CN) as a processing additive into the active layer. The high boiling point of CN (263 °C) and DIO (327 °C) reduce the evaporation kinetics in the blend solvent and should provide control over the morphology of the active layer [54]. Ca/Al contact was used in order to observe the effect of the additives on the donor–acceptor phase separation, which could eliminate the necessity of post annealing treatment.

The effect of a single additive (CN) was first studied (results not shown). The efficiency of the PV cells based on **PDTSDTBT-P2** decreased to 1.19% when 2.5% CN was used as a processing additive. A higher CN concentration (5% by volume) produced even larger **PDTSDTBT** aggregates, visible to naked eyes in the spincoat blend films, leading to a poorer device performance with a PCE of 1.05%.

Further investigations were done to evaluate the effect of the addition of DIO. The *J–V* curves are presented in Fig. 7 and device performance parameters are summarized in Table 6.

The results show that the **PDTSDTBT-P2** based device performance can be improved by the addition of DIO. The PCE of the PSC based on **PDTSDTBT-P2**:$PC_{60}BM$ (1:1 w/w) without any annealing treatment is 1.13%. The PCE was increased to 2.02% through the addition of 2% DIO into the

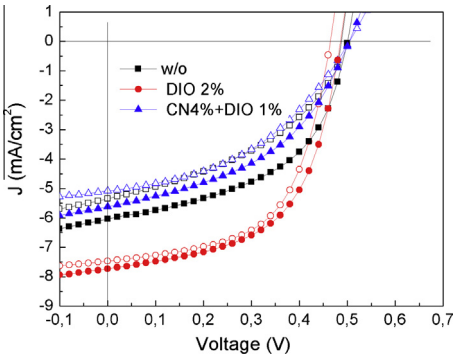

Fig. 7. *J–V* characteristics of polymer solar cells (ITO/PEDOT:PSS/**P2**:PC_{60}BM/Ca/Al) under AM1.5 solar illumination with and without additives. Open symbols indicate data without any annealing treatment and solid symbols represent data with pre-annealing of the films at 140 °C for 10 min.

Table 6
Device performance parameters of high molar mass **PDTSDTBT**:PC_{60}BM based solar cells (ITO/PEDOT:PSS/**P2**:PC_{60}BM /Ca/Al) prepared under different conditions.

Additives	PCE (%)	J_{SC} (mA cm^{-2})	V_{OC} (V)	FF (%)
–	1.13 (1.54[a])	5.35 (6.03[a])	0.48 (0.5[a])	44 (51[a])
2% DIO	2.02 (2.13[a])	7.47 (7.73[a])	0.46 (0.48[a])	59 (57[a])
4% CN + 1% DIO	1.11 (1.28[a])	5.08 (5.62[a])	0.50 (0.5[a])	44 (45[a])

[a] Films pre-annealed at 140 °C/10 min.

active layer with a V_{OC} = 0.46 V, a J_{SC} = 7.47 mA/cm^2 and a FF = 59%.

The increase of the PCE is mainly from the higher FF and J_{SC} attributed to the optimized phase separation of donor–acceptor. We also tried to use CN and DIO simultaneously as co-additives in the CB solution of **PDTSDTBT** and PC_{60}BM. The device prepared using 4% CN and 1% (v/v) DIO additives showed a J_{SC} of 5.08 mA/cm^2 and a FF of 44%, which are lower than the J_{SC} and FF obtained when we used 2% of DIO additive only. The addition of CN affects negatively the organization of the active layer and thus decreases solar cells performances based on **PDTSDTBT** copolymer. It is interesting to investigate the annealing effect on the active layers with or without additives. For that, films were pre-annealed at 140 °C for 10 min. Device without any additive show 35% of enhancement in PCE from 1.13% to 1.54%, while devices with DIO exhibit only 5% of increase from 2.02% to 2.13%, confirming that quite optimum donor–acceptor phase separation was already achieved with DIO as the only additive.

4. Conclusion

In summary, we designed a new low band gap polymer (**PDTSDTBT**) based on the DTS unit with linear octyl chains on the Si atom and introducing a thiophene spacer bearing a hexyl group at the β-position to study their effect on the conjugation length and photovoltaic performance. This DTS monomer with linear octyl chain was chosen on the basis of encouraging results and the cheap access to this monomer, compared to the one with branched chains. According to optical properties, increasing the molar mass of **PDTSDTBT** from 6600 g mol^{-1} (**P1**) to 15,700 g mol^{-1} (**P2**) causes an important red-shift of 44 nm due to higher conjugation length and lower band gap. This copolymer with both molar masses show better solubility with respect to **PDTSBT** as the π–π aggregation vibronic shoulder at 784 nm disappeared. However, the blue shift by 88 nm of the low energy band gap of **P1** with respect to **P3** reveals a twisting in the main backbone of the polymer that limits the intramolecular charge transfer. The E_g^{opt} values of **P1**, **P2** and **P3** are 1.56, 1.52 and 1.44 eV, respectively. Thermal analysis indicates a high thermal stability of the two copolymers that can be attributed to the presence of the aromatic ring dithieno[3,2-*b*:2′,3′-*d*]silole rich in silicon in the polymer backbone. The X-ray diffraction spectra indicate better crystallinity for the new copolymer as the diffraction peaks presented are up to third order. Regardless of the crystallinity, a higher π–π stacking distance for **PDTSDTBT** can indicate a twist in the main backbone due to steric hindrance of the hexyl group that reduce intramolecular charge transfer and limits the photovoltaic performance of the device. Although PSCs based on **P3** (PCE = 1.01%) performed better than **P1** (PCE = 0.61%) which has comparable molar mass, the highest PCE (1.41%) was achieved using higher molar mass **P2**. Both pre and post annealing treatment resulted in optimized device performance with PCE of 1.94%. The polymer showed superior device performance when PC_{60}BM was used as acceptor instead of PC_{70}BM thanks to its wide absorption profile. Without any annealing treatment, we have obtained PCE higher than 2% using Ca/Al as electron extracting contacts and 1,8-diiodooctane as processing additive.

Acknowledgments

The GIS Advanced Materials in Aquitaine is gratefully thanked for funding Hussein Medlej. This work has been supported by the French CNRS and the Région Aquitaine.

Appendix A. Supplementary material

TGA plots of PDTSDTBT and PDTSBT, DSC thermograms of PDTSDTBT and PDTSBT and CV oxidation and reduction curves of PDTSDTBT and CV curve of ferrocene.

Supplementary data associated with this article can be found, in the online version, at http://dx.doi.org/10.1016/j.eurpolymj.2013.09.025.

References

[1] Solomon S, Plattner GK, Knutti R, Friedlingstein P. Irreversible climate change due to carbon dioxide emissions. Proc Natl Acad Sci USA 2009;106:1704–9.
[2] Goetzberger A, Hebling C, Schock HW. Photovoltaic materials, history, status and outlook. Mater Sci Eng R 2003;40:1–46.
[3] Padinger F, Rittberger RS, Sariciftci NS. Effects of postproduction treatment on plastic solar cells. Adv Funct Mater 2003;13:85–8.
[4] Dang MT, Hirsch L, Wantz G. P3HT:PCBM, best seller in polymer photovoltaic research. Adv Mater 2011;23:3597–602.
[5] (a) Li Y. Molecular design of photovoltaic materials for polymer solar cells: towards suitable electronic energy levels and broad absorption. Acc Chem Res 2012;45:723–33;

(b) Zhang Z-G, Wang J. Structures and properties of conjugated donor–acceptor copolymers for solar cell applications. J Mater Chem 2012;22:4178–87;
(c) Gendron D, Leclerc M. New conjugated polymers for plastic solar cells. Energy Environ Sci 2011;4:1225–37.
[6] Søndergaard RR, Hösel M, Krebs FC. Roll-to roll fabrication of large area functional organic materials. J Polym Sci B: Polym Phys 2013;51:16–34.
[7] (a) Pron A, Berrouard P, Leclerc M. Thieno[3,4-c]pyrrole-4,6-dione-based polymers for opto-electronic applications. Macromol Chem Phys 2013;214:7–16;
(b) Small CE, Chen S, Subbiah J, Amb CM, Tsang SW, Lai TH, et al. High-efficiency inverted dithienogermole-thienopyrrolodione-based polymer solar cells. Nat Photon 2012;6:115–20.
[8] Nelson J. Polymer:fullerene bulk heterojunction solar cells. Mater Today 2011;14:462–70.
[9] Green MA, Emery K, Hishikawa Y, Warta W, Dunlop ED. Solar cell efficiency tables (version 39). Prog Photovolt: Res Appl 2012;20:12–20.
[10] Roncali J. Synthetic principles for bandgap control in linear π-conjugated systems. Chem Rev 1997;97:173–206.
[11] Roncali J. Molecular engineering of the band gap of π-conjugated systems: facing technological applications. Macromol Rapid Commun 2007;28:1761–75.
[12] Havinga E, Hoeve W, Wynberg H. A new class of small band gap organic polymer conductors. Polym Bull 1992;29:119–26.
[13] Bijleveld JC, Zoombelt AP, Mathijssen SGJ, Wienk MM, Turbiez M, de Leeuw DM, et al. Poly(diketopyrrolopyrrole-terthiophene) for ambipolar logic and photovoltaics. J Am Chem Soc 2009;131:16616–7.
[14] Park SH, Roy A, Beaupré S, Cho S, Coates N, Moon JS, et al. Bulk heterojunction solar cells with internal quantum efficiency approaching 100%. Nat Photonics 2009;3:297–302.
[15] Slooff LH, Veenstra SC, Kroon JM, Moet DJD, Sweelssen J, Koetse MM. Determining the internal quantum efficiency of highly efficient polymer solar cells through optical modeling. Appl Phys Lett 2007;90:143506/1–6/3.
[16] Wang E, Wang L, Lan L, Luo C, Zhuang W, Peng J, et al. High-performance polymer heterojunction solar cells of a polysilafluorene derivative. Appl Phys Lett 2008;92:033307/1–7/3.
[17] Chu TY, Lu J, Beaupre S, Zhang Y, Pouliot JR, Wakim S, et al. Bulk heterojunction solar cells using thieno[3,4-c]pyrrole-4,6-dione and dithieno[3,2-b:2′,3′-d]silole copolymer with a power conversion efficiency of 7.3%. J Am Chem Soc 2011;133:4250–3.
[18] Piliego C, Holcombe TW, Douglas JD, Woo CH, Beaujuge PM, Fréchet JMJ. Synthetic control of structural order in N-alkylthieno[3,4-c]pyrrole-4,6-dione-based polymers for efficient solar cells. J Am Chem Soc 2010;132:7595–7.
[19] Peet J, Kim JY, Coates NE, Ma WL, Moses D, Heeger AJ, et al. Efficiency enhancement in low-bandgap polymer solar cells by processing with alkane dithiols. Nat Mater 2007;6:497–500.
[20] Coffin RC, Peet J, Rogers J, Bazan GC. Streamlined microwaveassisted preparation of narrow-bandgap conjugated polymers for high-performance bulk heterojunction solar cells. Nat Chem 2009;1:657–61.
[21] Bijleveld JC, Gevaerts VS, Nuzzo DD, Turbiez M, Mathijssen SGJ, de Leeuw DM, et al. Efficient solar cells based on an easily accessible diketopyrrolopyrrole polymer. Adv Mater 2010;22:E242–6.
[22] Chen HY, Hou J, Zhang S, Liang Y, Yang G, Yang Y, et al. Polymer solar cells with enhanced open-circuit voltage and efficiency. Nat Photonics 2009;3:649–53.
[23] Huo L, Chen HY, Hou J, Chen TL, Yang Y. Low band gap dithieno[3,2-b:2′,3′-d]silole-containing polymers, synthesis, characterization and photovoltaic application. Chem Commun 2009;37:5570–2.
[24] Hou J, Chen HY, Zhang S, Li G, Yang Y. Synthesis, characterization, and photovoltaic properties of a low band gap polymer based on silole-containing polythiophenes and 2,1,3-benzothiadiazole. J Am Chem Soc 2008;130:16144–5.
[25] (a) Zhang M, Guo X, Li Y. Synthesis and characterisation of a copolymer based on thiazolothiazole and dithienosilole for polymer solar cells. Adv Energy Mater 2011;1:557–60;
(b) Cui C, Fan X, Zhang M, Zhang J, Min J, Li Y. A D–A copolymer of dithienosilole and a new acceptor unit of naphto[2,3-c]thiophene-4,9-dione for efficient polymer solar cells. Chem Commun 2011;47:11345–7.
[26] Manceau M, Bundgaard E, Carlé JE, Hagemann O, Helgesen M, Sondergaard R, et al. Photochemical stability of π-conjugated polymers for polymer solar cells: a rule of thumb. J Mater Chem 2011;21:4132–41.
[27] (a) Risko C, Kushto GP, Kafafi ZH, Brédas JL. Electronic properties of silole-based organic semiconductors. J Chem Phys 2004;121:9031–8;
(b) Yamaguchi S, Tamao K. Theoretical study on the electronic structure of 2,2′-bisilole in comparison with 1,1′-bicyclopentadiene:s*-p* conjugation and low-lying lumo as the origin of unusual optical properties of 3,3′,4,4′-tetraphenyl-2,2′-bisilole. Bull Chem Soc Jpn 1996;69:2327–34.
[28] Mühlbacher D, Scharber M, Morana M, Zhu Z, Waller D, Gaudiana R, et al. High photovoltaic performance of a low-bandgap polymer. Adv Mater 2006;18:2884–9.
[29] Neto BAD, Lopes AS, Wust M, Costa VEU, Ebeling G, Dupont J. Tetrahedron Lett 2005;46:6843–6.
[30] (a) Allard N, Aich RB, Gendron D, Boudreault P-LT, Tessier C, Alem S, et al. Germafluorenes: new heterocycles for plastic electronics. Macromolecules 2010;43:2328–33;
(b) Lu J, Liang F, Drolet N, Ding J, Tao Y, Movileanu R. Crystalline low band-gap alternating indolocarbazole and benzothiadiazole-cored oligothiophene copolymer for organic solar cell applications. Chem Commun 2008;42:5315–7.
[31] Zhan X, Risko C, Amy F, Chan C, Zhao W, Barlow S, et al. Electron affinities of 1,1-diaryl-2,3,4,5-tetraphenylsiloles: direct measurements and comparison with experimental and theoretical estimates. J Am Chem Soc 2005;127:9021–9.
[32] (a) Nguyen LH, Gunes S, Neugebauer H, Sariciftci NS, Colladet K, Fourier S, et al. Side chain effects on photoinduced absorption and photovoltaic performance of low bandgap thienylene vinylene and phenylene vinylene copolymers. Eur Phys J Appl Phys 2006;36:219–24;
(b) Li W, Qin R, Zhou Y, Andersson M, Li F, Zhang C, et al. Tailoring side chains of low band gap polymers for high efficiency polymer solar cells. Polymer 2010;51:3031–8.
[33] Liao L, Dai L, Smith A, Durstock M, Lu J, Ding J, et al. Photovoltaic-active dithienosilole-containing polymers. Macromolecules 2007;40:9406–12.
[34] Helgesen M, Sorensen TJ, Manceau M, Krebs FC. Photochemical stability and photovoltaic performance of low-band gap polymers based on dithiophene with different bridging atoms. Polym Chem 2011;2:1355–61.
[35] Biniek L, Fall S, Chochos CL, Anokhin DV, Ivanov DA, Leclerc N, et al. Impact of the alkyl side chains on the optoelectronic properties of a series of photovoltaic low-band-gap copolymers. Macromolecules 2010;43:9779–86.
[36] Lee SK, Cho S, Tong M, Seo JH, Heeger AJ. Effects of substituted side-chain position on donor–acceptor conjugated copolymers. J Polym Sci A: Polym Chem 2011;49:1821–9.
[37] Daasbjerg K, Pedersen SU, Lund H. In: Alfassi ZB, editor. General aspects of the chemistry of radicals. Chichester, UK: Wiley; 1999. p. 385–427.
[38] Liu J, Zhang R, Sauve G, Kowalewski T, McCullough RD. Highly disordered polymer field effect transistors: *n*-alkyl dithieno[3,2-*b*:2′,3′-*d*]pyrrole-based copolymers with surprisingly high charge carrier mobilities. J Am Chem Soc 2008;130:13167–76.
[39] Bundgaard E, Krebs FC. Macromolecules 2006;39:2823–31.
[40] Tierney S, Heeney M, McCulloch I. Microwave-assisted synthesis of polythiophenes via the Stille coupling. Synth Met 2005;148:195–8.
[41] Jesperse KG, Beenken WJD, Zaushitsyn Y, Yartsev A, Andersson MR, Pullerits T, et al. The electronic states of polyfluorene copolymers with alternating donor–acceptor units. J Chem Phys 2004;121:12613–7.
[42] Roquet S, Cravino A, Leriche P, Aléveque O, Frère P, Roncali J. Triphenylamine–thienylenevinylene hybrid systems with internal charge transfer as donor materials for heterojunction solar cells. J Am Chem Soc 2006;128:3459–66.
[43] Chen H-Y, Hou J, Hayden AE, Yang H, Houk KN, Yang Y. Silicon atom substitution enhances interchain packing in a thiophene-based polymer system. Adv Mater 2010;22:371–5.
[44] Li G, Shrotriva V, Huang JS, Yao Y, Moriarty T, Emery K, et al. High-efficiency solution processable polymer photovoltaic cells by self-organization of polymer blends. Nat Mater 2005;4:864–8.
[45] Yuan M-C, Chou Y-J, Chen C-M, Hsu C-L, Wei K-H. A crystalline low-bandgap polymer comprising dithienosilole and thieno[3,4-*c*]pyrrole-4,6-dione units for bulk heterojunction solar cells. Polymer 2011;52:2792–8.
[46] Chen H-Y, Hou J, Hayden AE, Yang H, Houk KN, Yang Y. Efficient polymer solar cells with thin active layers based on alternating

polyfluorene copolymer/fullerene bulk heterojunctions. Adv Mater 2009;21:4239–42.
[47] Brinkmann M. Structure and morphology control in thin films of regioregular poly(3-hexylthiophene). J Polym Sci B: Polym Phys 2011;49:1218–33.
[48] Kaynkid N, Uttiya S, Brinkmann M. Structural model of regioregular poly(3-hexylthiophene) obtained by electron diffraction analysis. Macromolecules 2010;43:4961–7.
[49] Beal RM, Stavrinadis A, Warner JH, Smith JM, Assender HE, Watt AAR. The molecular structure of polymer–fullerene composite solar cells and its influence on device performance. Macromolecules 2010;43:2343–8.
[50] Brédas JL, Silbey R, Bourdreaux DS, Chance RR. Chain-length dependence of electronic and electrochemical properties of conjugated systems: polyacetylene, polyphenylene, polythiophene, and polypyrrole. J Am Chem Soc 1983;105:6555–9.
[51] He YJ, Li YF. Fullerene derivative acceptors for high performance polymer solar cells. Phys Chem Chem Phys 2011;13:1970–83.
[52] Chu T-Y, Lu J, Beaupré S, Zhang Y, Pouliot J-R, Zhou J, et al. Effects of the molecular weight and the side-chain length on the photovoltaic performance of dithienosilole/thienopyrrolodione copolymers. Adv Funct Mater 2012;22:2345–51.
[53] (a) Liu B, Chen X, Zou Y, He Y, Xiao L, Xu X, et al. A benzo[1,2-*b*:4,5-*b*′]difuran- and thieno-[3,4-*b*]thiophene-based low bandgap copolymer for photovoltaic applications. Polym Chem 2013;4:470–6;
(b) Liang Y, Xu Z, Xia J, Tsai ST, Wu Y, Li G, et al. For the bright future—bulk heterojunction polymer solar cells with power conversion efficiency of 7.4%. Adv Mater 2010;22:E135–8;
(c) Jo J, Gendron D, Najari A, Moon JS, Cho S, Leclerc M, et al. Bulk heterojunction solar cells based on a low-bandgap carbazole-diketopyrrolopyrrole copolymer. Appl Phys Lett 2010;97:203303;
(d) Moon JS, Takacs CJ, Cho S, Coffin RC, Kim H, Bazan GC, et al. Effect of processing additive on the nanomorphology of a bulk heterojunction material. Nano Lett 2010;10:4005–8.
[54] Hoven CV, Dang X-D, Coffin RC, Peet J, Nguyen T-Q, Bazan GC. Improved performance of polymer bulk heterojunction solar cells through the reduction of phase separation via solvent additives. Adv Mater 2010;22:E63–6.